

Chirality Breaking of Majorana Edge Modes Induced by Chemical Potential Shifts

Xin Yue^{1,*} and Guo-Jian Qiao²

¹Beijing Computational Science Research Center, Beijing 100193, China

²Graduate School of China Academy of Engineering Physics, Beijing 100193, China

(Dated: March 9, 2026)

Quantum anomalous Hall insulator-superconductor heterostructures are predicted to host chiral Majorana fermions as edge modes, which is essential for topological quantum computing applications. Although the edge states have been extensively studied at zero chemical potential $\mu = 0$, the practically relevant regime with a shifted chemical potential ($\mu \neq 0$) remains less explored. Here, we present an analytical treatment of the edge states for $\mu \neq 0$, deriving an approximate but highly accurate solution applicable to realistic experimental parameters. Surprisingly, we find that the energy dispersion of the edge band exhibits nonlinearity and transforms into a twisted, braid-like structure within specific parameter ranges. This unique braid-like band leads to non-chirality of the edge modes, allowing propagation in both directions.

I. INTRODUCTION

Majorana fermions, proposed in 1937 by Ettore Majorana, are exotic particles that are their own antiparticles [1]. In condensed matter physics, the quasi-excitations including Majorana zero modes and chiral Majorana fermion modes, have been extensively studied theoretically [2–24] and experimentally [25–31] due to their exotic properties and potential applications in fault-tolerant quantum computing [32–36].

The chiral Majorana fermion, as a quasiparticle, can be realized at the edge of 2D topological materials [2]. Specifically, heterostructures [4] composed of a quantum anomalous Hall (QAH) insulator and an s -wave superconductor are considered as a promising platform to host Majorana edge modes [6]. These modes propagate along the edges unidirectionally [see Fig. 1(a)], which is why they are referred to as chiral Majorana fermion modes or chiral Majorana edge modes [6, 10, 14, 36].

These edge modes in heterostructure were studied in the special case where the effective chemical potential of the QAH insulator is zero, $\mu = 0$ [6, 19]. In this scenario, the edge states exhibit a linear dispersion relation, as shown in Fig. 1(b). However, in practical experimental realizations, the chemical potential in the topological insulator layer is often shifted due to finite-size effect of the superconductor [18–20, 37–39]. Therefore, it is necessary to study the edge states of this system when μ is not zero.

In this paper, we investigate the edge states in the quantum anomalous Hall (QAH)-superconductor heterostructure for non-zero chemical potential ($\mu \neq 0$). While the formalism for analyzing edge states in topological systems is well-established [40–43], previous studies have typically involved solving quadratic equations to determine the decay length of edge states. However, when $\mu \neq 0$, the primary challenge lies in solving a quartic equation to address the decay length problem. To over-

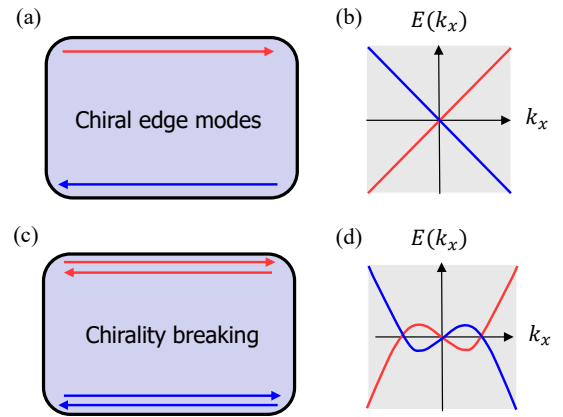


FIG. 1. (a) Illustration of chiral Majorana fermion propagating at the edge of 2D material, and (b) linear energy dispersion of the edge states. The 2D material could be 2D p -wave superconductor [2], or heterostructure form by QAH insulator and s -wave superconductor [6]. (c) Illustration for the chirality-breaking of Majorana edge modes under chemical potential shift. (d) The dispersion relation of edge states shows a twisted, braid-like shape so that each edge band intersect Fermi level three times.

come this, we present an analytical approach that yields highly accurate solutions across physically relevant parameter ranges, which are further validated by numerical calculations. Remarkably, the Majorana edge mode loses its chiral nature within specific regions of parameter space. In these regions, the energy dispersion of the edge states $E(k_x)$ becomes nonlinear and can exhibit a twisted, braid-like shape [see Fig. (d)]. This dispersion develops a kink such that the edge states intersect the Fermi level three times: twice with a positive group velocity and once with a negative group velocity [44, 45] and consequently lose their chiral nature [see Fig. (c)]. The parameter region in which this braid-like edge state emerges is further determined using the analytical approach. Consequently, caution should be exercised when referring to “chiral Majorana fermions” at nonzero chem-

* Contact author: yuexin@csrc.ac.cn

ical potential.

II. EDGE STATES UNDER CHEMICAL POTENTIAL SHIFT

The QAH-superconductor heterostructure can be described by a Bogoliubov-de Gennes Hamiltonian in momentum space [6, 10]:

$$\mathcal{H}(\mathbf{k}) = \begin{pmatrix} h_Q(\mathbf{k}) - \mu & \Delta \\ \Delta^\dagger & -h_Q^*(-\mathbf{k}) + \mu \end{pmatrix}, \quad (1)$$

where the Hamiltonian of the QAH insulator is [46]

$$h_Q(\mathbf{k}) = A(k_x\sigma_x + k_y\sigma_y) + (m - Bk^2)\sigma_z, \quad (2)$$

and Δ denotes the superconducting pairing in the QAH insulator induced by the proximity effect. Here, $\mathbf{k} = (k_x, k_y)$ is the electron momentum, μ is the chemical potential, σ_i ($i = x, y, z$) is the Pauli matrices, and A, B and m are material-specific parameters.

We consider a semi-infinite plane ($y \geq 0$) with open boundary conditions along the y direction and translational invariance along x . Under this geometry, k_x remains a good quantum number, denoted as k_x , while k_y is replaced by the differential operator $-i\partial_y$. Then the eigenvalue equation becomes

$$\mathcal{H}(k_x, -i\partial_y) \Psi_{k_x}(y) = E \Psi_{k_x}(y). \quad (3)$$

To search for zero-energy modes localized at the edge $y = 0$, we first focus on the $k_x = 0$ and $E = 0$ case. A localized ansatz can be written as

$$\Psi_{k_x}(y) = e^{-\xi y} \begin{pmatrix} \mathbf{u}_{k_x} \\ \mathbf{v}_{k_x} \end{pmatrix}, \quad (4)$$

where $\text{Re}(\xi) > 0$ ensures decay as $y \rightarrow \infty$.

A. Decay lengths and Wave Functions

The characteristic equation $\det[\mathcal{H}(0, i\xi)] = 0$ yields eight solutions for the decay length ξ . Considering that B is small in practical material, the approximate solutions are obtained as follows (see Appendix A for detailed derivation):

1. Neglating B directly, we obtain four solutions:

$$\xi_{1,2} \approx \frac{\Delta \pm \sqrt{m^2 - \mu^2}}{A}, \quad \xi_{3,4} \approx -\frac{\Delta \pm \sqrt{m^2 - \mu^2}}{A}. \quad (5)$$

In fact, the presence of B only leads to a small correction to these solutions.

2. Four additional solutions are

$$\xi_{5,6} \approx \pm \frac{A}{B}, \quad \xi_{7,8} \approx \pm \frac{A}{B}. \quad (6)$$

These solutions are much larger than the previous four because B is small.

The corresponding un-normalized wave functions are:

$$\begin{aligned} \Psi_1 &= e^{-\xi_1 y}(\sigma, -1, -\sigma, 1)^T, & \Psi_2 &= e^{-\xi_2 y}(\sigma, 1, -\sigma, -1)^T, \\ \Psi_3 &= e^{-\xi_3 y}(\sigma, 1, \sigma, 1)^T, & \Psi_4 &= e^{-\xi_4 y}(\sigma, -1, \sigma, -1)^T, \\ \Psi_5 &= e^{-\xi_5 y}(1, 1, 1, 1)^T, & \Psi_6 &= e^{-\xi_6 y}(1, -1, 1, -1)^T, \\ \Psi_7 &= e^{-\xi_7 y}(1, 1, -1, -1)^T, & \Psi_8 &= e^{-\xi_8 y}(1, -1, -1, 1)^T, \end{aligned}$$

where $\sigma \equiv (m + \mu)/\sqrt{m^2 - \mu^2}$.

B. Boundary Conditions and Eigenstates

The edge states must satisfy the boundary conditions $\Psi(y = 0) = 0$ and $\Psi(y \rightarrow \infty) = 0$. Therefore, only solutions with $\text{Re}(\xi) > 0$ are physically admissible when considering edge modes localized near $\Psi(y = 0) = 0$. Furthermore, to satisfy the boundary condition at $y = 0$, the edge states must be constructed as a linear combination of these admissible solutions.

In the parameter regime $|m| < \sqrt{\Delta^2 + \mu^2}$, with $A, B > 0$, it follows that $\text{Re}(\xi_1), \text{Re}(\xi_2) > 0$ and $\xi_5 = \xi_7 = A/B > 0$, while the remaining roots possess a negative real part and correspond to non-physical growing modes. Consequently, a trial wavefunction can be written as:

$$\Psi(y) = c_1 \Psi_1(y) + c_2 \Psi_2(y) + c_5 \Psi_5(y) + c_7 \Psi_7(y), \quad (7)$$

where $\Psi_{1,2,5,7}(y)$ are eigenstate solutions associated with the positive roots. The boundary condition $\Psi(0) = 0$ leads to the following set of equations:

$$\begin{aligned} (c_1 + c_2)\sigma + c_5 + c_7 &= 0, & -c_1 + c_2 + c_5 + c_7 &= 0, \\ -(c_1 + c_2)\sigma + c_5 - c_7 &= 0, & c_1 - c_2 + c_5 - c_7 &= 0. \end{aligned}$$

By setting $c_7 = -1$, one obtains:

$$c_1 = \frac{1 - \sigma}{2\sigma}, \quad c_2 = \frac{1 + \sigma}{2\sigma}, \quad c_5 = 0. \quad (8)$$

It is straightforward to verify from Eqs.(7) and (8) that the electron and hole components of the wave function satisfy $\Psi_{e\uparrow} = \Psi_{h\uparrow}$. This property originates from the particle-hole symmetry of the system and indicates that the edge mode is a Majorana-type mode.

C. Edge States in Different Chemical Potential

In the above analysis, the general form of the edge state wavefunction was derived under the conditions $|m| < \sqrt{\Delta^2 + \mu^2}$ and $k_x = 0$. In this section, we present explicit expressions for the edge states in different chemical potential regimes.

(i) For $|\mu| < |m|$, the electron components of the edge-state wave function are given by:

$$\begin{aligned} \Psi_{e\uparrow} &= \frac{1+p}{2} e^{-\frac{\Delta-s}{A}y} + \frac{1-p}{2} e^{-\frac{\Delta+s}{A}y} - e^{-\frac{A}{B}y}, \\ \Psi_{e\downarrow} &= \frac{1+p}{2p} e^{-\frac{\Delta-s}{A}y} + \frac{1-p}{2p} e^{-\frac{\Delta+s}{A}y} - e^{-\frac{A}{B}y}, \end{aligned}$$

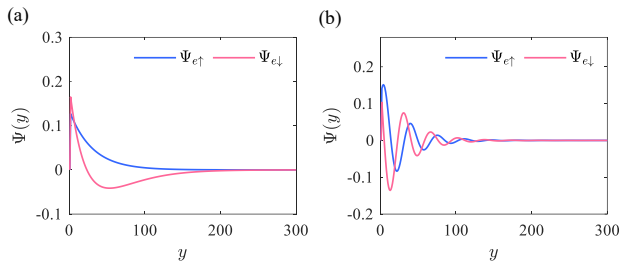


FIG. 2. Edge state wave function under a chemical potential shift. Only the electron component is displayed, as the hole component is identical to the electron component. (a) $|\mu| = |m|$, where the spin-up component of the edge state $\Psi_{e\uparrow}$ decays exponentially, while the spin-down component $\Psi_{e\downarrow}$ exhibits an exponential decay modified by a linear factor $(1 + \frac{2m}{A}y)$. (b) $|\mu| > |m|$, where the edge states oscillate and decay simultaneously.

with $p \equiv (m + \mu)/S$ and $S \equiv \sqrt{m^2 - \mu^2}$.

(ii) For $|\mu| > |m|$, the edge state wave function exhibits oscillatory decay, as shown in Fig. 2(b). Specifically, one finds:

$$\begin{aligned}\Psi_{e\uparrow} &= \cos\left(\frac{Qy}{A}\right) e^{-\frac{\Delta}{A}y} + \frac{m + \mu}{Q} \sin\left(\frac{Qy}{A}\right) e^{-\frac{\Delta}{A}y} - e^{-\frac{A}{B}y}, \\ \Psi_{e\downarrow} &= \cos\left(\frac{Qy}{A}\right) e^{-\frac{\Delta}{A}y} - \frac{Q}{m + \mu} \sin\left(\frac{Qy}{A}\right) e^{-\frac{\Delta}{A}y} - e^{-\frac{A}{B}y},\end{aligned}$$

where $Q \equiv \sqrt{\mu^2 - m^2}$. These solutions describe oscillatory Majorana edge states in the regime where the chemical potential exceeds the effective mass gap.

(iii) When $\mu = -m$, a limiting procedure can be employed to derive the explicit wavefunction forms. The resulting components are:

$$\Psi_{e\uparrow} = e^{-\frac{\Delta}{A}y} - e^{-\frac{A}{B}y}, \quad (9)$$

$$\Psi_{e\downarrow} = \left(1 + \frac{2m}{A}y\right) e^{-\frac{\Delta}{A}y} - e^{-\frac{A}{B}y}. \quad (10)$$

In this case, both the spin-up and spin-down components of the edge state decay exponentially [see Fig. 2(a)].

(iv) When $\mu = 0$ and $m < 0$, the wavefunction Ψ simplifies to a linear combination of two basis states, consistent with the edge-state solutions commonly presented in the literature for systems such as the quantum spin Hall insulator [40, 43, 47], topological insulator Be_2Se_3 [41] and the lattice model of a 1D p -wave superconductor [3]. Specifically:

$$\Psi_{e\uparrow} = \Psi_{e\downarrow} = e^{-\frac{y(\Delta - m)}{A}} - e^{-\frac{yA}{B}}. \quad (11)$$

These expressions demonstrate the distinctive decay behavior of the edge states in different chemical potential shift regime.

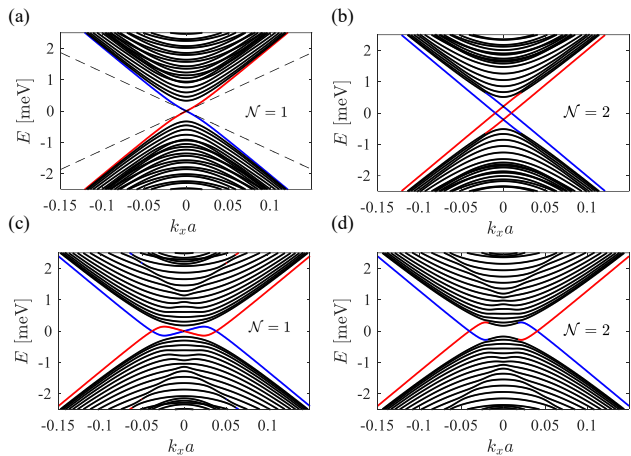


FIG. 3. Energy spectra of the heterostructure system with various parameters. The edge bands are highlighted in red and blue. (a) $m = -0.6$ meV, $\mu = 1$ meV. (b) $m = 2$ meV, $\mu = 0.5$ meV. (c) $m = -2$ meV, $\mu = 2$ meV, where the edge bands form a braid-like structure. (d) $m = -2.5$ meV, $\mu = 2$ meV. Other parameters are identical for (a-d): $\Delta_s = 1$ meV, $A = 0.3$ meV $\cdot \mu\text{m}$, and $B = 1.5 \times 10^{-4}$ meV $\cdot \mu\text{m}^2$, with a lattice constant $a = 5$ nm and a length $L_y = N_y a = 2 \mu\text{m}$ along the y direction.

III. ENERGY BAND STRUCTURE UNDER CHEMICAL POTENTIAL SHIFT

Due to the presence of proximity-induced pairing in the QAH system, the bands do not simply shift uniformly when the chemical potential μ is varied, particularly for the edge states. To explore this behavior quantitatively, we map the continuous model onto a discrete lattice. The energy spectra are obtained by numerically diagonalizing the Hamiltonian [6, 42, 43], with open boundary conditions along the y -direction and periodic boundary conditions along the x -direction.

Under these boundary conditions, the wave function of the bulk states generally takes the form $\psi \sim \exp(ik_x x) \sin(k_y y)$, while the wave function of the edge states generally takes the form $\psi \sim \exp(ik_x x) \exp(-\xi y)$. Therefore, the edge and bulk states can be distinguished by analyzing the spatial distribution of the eigenstates. Specifically, if the majority of the wave function (set to 80%) is localized on the $y = 0$ boundary, it is identified as a edge state and marked with red dots in Fig. 3. If the majority of the wave function is localized on the $y = L_y$ boundary, it is identified as a edge state and marked with blue dots. If neither condition is satisfied, the state is considered a bulk state and marked with black dots (see Fig. 3).

For the $\mathcal{N} = 2$ topological phase (defined by $m < -\sqrt{\Delta^2 + \mu^2}$) [6, 10], we observe two edge bands on each side. These edge bands shift collectively as the chemical potential varies. In contrast, for the $\mathcal{N} = 1$ topological phase (defined by $|m| < \sqrt{\Delta^2 + \mu^2}$) [6, 10], only one edge

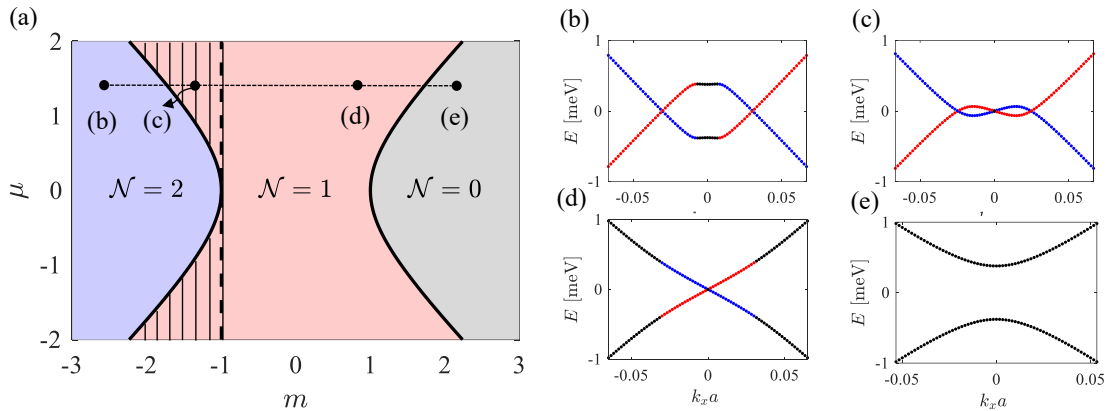


FIG. 4. This figure illustrates the topological phase diagram as a function of m and μ , with the shaded regions representing areas where braid-like edge bands emerge. Panels (b)-(e) correspond to energy spectra at specific parameter sets labeled in (a), only the lowest band is shown for clarity. Other parameter are setting the same as that in Fig. 3.

band exists on each side, and its position is not affected by changes in the chemical potential. Interestingly, we find that in certain parameter regimes, the edge bands form a braid-like structure, as shown in Fig. 3(c). A natural question is what parameter range gives rise to this braid-like dispersion of the edge state.

IV. CONDITIONS FOR THE EMERGENCE OF BRAID-LIKE BANDS

As shown above, the dispersion of the edge states can exhibit a braid-like structure under specific parameter settings. To determine the origin of these exotic structure, we examine the edge-state dispersion under perturbation by small k_x . For $k_x \neq 0$, the Hamiltonian can be decomposed as

$$\mathcal{H}(k_x, -i\partial_y) = \mathcal{H}_0(-i\partial_y) + \mathcal{H}_1(k_x), \quad (12)$$

where the perturbative term $\mathcal{H}_1(k_x)$ is expressed as

$$\mathcal{H}_1(k_x) = \begin{pmatrix} Bk_x^2 & Ak_x & 0 & 0 \\ Ak_x & -Bk_x^2 & 0 & 0 \\ 0 & 0 & -Bk_x^2 & Ak_x \\ 0 & 0 & Ak_x & Bk_x^2 \end{pmatrix}. \quad (13)$$

To first order in k_x , the group velocity v of edge modes can be derived from standard perturbation theory. Using the wave function $\Psi(y) = c_1 \mathbf{v}_1 e^{-\xi_1 y} + c_2 \mathbf{v}_2 e^{-\xi_2 y} + c_7 \mathbf{v}_7 e^{-\xi_7 y}$ for edge states, the dispersion energy $E(k_x)$ is given by

$$\begin{aligned} E(k_x) &= \int_0^\infty dy \Psi^\dagger(y) \mathcal{H}_1(k_x) \Psi(y) \\ &= \sum_{i,j=1,2,7} c_i^* c_j \left(\mathbf{v}_i^\dagger \mathcal{H}_1(k_x) \mathbf{v}_j \right) I_{ij}, \end{aligned} \quad (14)$$

where $\mathbf{v}_i = \Psi_i e^{\xi_i y}$ and $I_{ij} = \int_0^\infty e^{-\xi_i^* y} e^{-\xi_j y} dy = 1/(\xi_i^* + \xi_j)$ represents overlap integrals stemming from the edge-state wave functions. Since B is typically small for realistic materials, terms involving \mathbf{v}_7 (corresponding to $\xi_7 = A/B \gg \xi_1, \xi_2$) can be neglected. This greatly simplifies the result to the following dispersion relation [see Appendix B for calculation details]:

$$E(k_x) = \frac{\Delta^2 + m\Delta}{\Delta^2 + m\Delta + \mu^2} Ak_x. \quad (15)$$

This analytical expression is consistent with numerical results obtained from diagonalizing the lattice model. For $\mu = 0$ (corresponding to $\sigma = 1$), the results reproducing the linear dispersion Ak_x reported widely in studies of topological edge states [6, 42].

It is worth noting that the dispersion relation Eq. (15) is only applicable in the topological region $\mathcal{N} = 1$, since our calculation starts from the eigenvalue $E(k_x = 0) = 0$. This eigenvalue ceases to exist when $\mathcal{N} = 2$, and therefore the above calculation does not apply. In the $\mathcal{N} = 2$ case, the two edge bands at one side shift by the chemical potential as $E = Ak_x \pm \mu$ in the perturbative sense. When the system undergoes a phase transition from $\mathcal{N} = 2$ to $\mathcal{N} = 1$, the two separated shifted edge bands fuse into a single band, forming an N -shaped curve with linear asymptotes. The N -shaped curves (red) and inverted N -shaped curves (blue) intertwine with each other, resembling a braid [see Fig. 4(c)].

The critical point where the N -shaped curve appears corresponds to where the slope of the dispersion at $k_x = 0$ vanishes. It follows from Eq. (15) that the critical condition is $\Delta + m = 0$. When $\Delta + m < 0$, the numerator of the dispersion relation becomes negative, while the denominator is always positive in the $\mathcal{N} = 1$ region. Therefore, the region defined by $\Delta + m < 0$ and $m > -\sqrt{\Delta^2 + \mu^2}$ corresponds to the parameter regime where the braid-like edge bands emerge, as illustrated by the shaded region in Fig. 4(a).

V. NON-CHIRALITY IN THE BRAID-LIKE BAND

A. What is chirality?

Chirality in edge transport refers to the presence of modes that propagate only in one direction without counter-propagating partners. A paradigmatic example can be found in the edge mode of a quantum Hall state [44, 48], a quantum anomalous Hall state [46, 49] or a two-dimensional p -wave superconductor [2], characterized by the linear dispersion $E(k_x) = Ak_x$. The group velocity $v_g = \partial E / \partial k_x = A$ is constant, indicating that all excitations propagate uniformly in the same direction.

To explicitly describe the motion of the Majorana edge modes, we consider an initial wave packet composed of edge eigenstates localized at the boundary, with momentum components drawn from the dispersion relation:

$$\Psi(x, y) = \int dk_x g(k_x) e^{ik_x x} \Psi_{k_x}(y), \quad (16)$$

where $g(k_x)$ is a Gaussian distribution centered at a chosen k_0 , and $\Psi_{k_x}(y)$ are the edge states. During time evolution, the group velocity $v_g(k_x) = dE/dk_x$ governs the propagation speed of the wavepacket center. For a band with linear dispersion [see Fig. 1(b)], the sign of v_g is fixed as k_x varies, ensuring the wavepacket propagates in a single direction.

B. Why are the braid-like edge bands non-chiral?

The braid-like edge bands discussed previously exhibit a distinctly different behavior due to their nonlinear dis-

person structure. In such bands, the group velocity $v_g(k_x) = dE/dk_x$ becomes a non-monotonic function, changing sign at certain points within the Brillouin zone [see Fig. 1(d)].

This non-monotonicity has profound consequences for wavepacket propagation. As the wavepacket evolves, portions corresponding to positive slopes propagate forward (right-moving), while portions corresponding to negative slopes propagate backward (left-moving). This division results in the splitting of the wavepacket, rather than a unidirectional propagation. Furthermore, at the momentum points where $dE/dk_x = 0$, the group velocity vanishes, causing the center of the wavepacket to hold during its propagation.

ACKNOWLEDGMENTS

The authors are grateful to C.P. Sun for drawing their attention to this question. This study was supported by the Science Challenge Project (Grant No. TZ2025017), the National Natural Science Foundation of China (NSFC) (Grant No. 12088101, 12547124), and the China Postdoctoral Science Foundation (Grant No. 2025M784438).

DATA AVAILABILITY

The data that support the findings of this article are not publicly available. The data are available from the authors upon reasonable request.

Appendix A: Detailed Derivation of Decay lengths

The BdG matrix for the $k_x = 0$ case with $k_y \rightarrow i\xi$ reads:

$$\mathcal{H}(0, i\xi) = \begin{pmatrix} -B\xi^2 + m - \mu & A\xi & 0 & \Delta \\ -A\xi & B\xi^2 - m - \mu & -\Delta & 0 \\ 0 & -\Delta & B\xi^2 - m + \mu & -A\xi \\ \Delta & 0 & A\xi & -B\xi^2 + m + \mu \end{pmatrix}. \quad (A1)$$

The determinant factorization gives: $\det[\mathcal{H}(0, i\xi)] = F_1(\xi)F_2(\xi)$, where

$$F_1(\xi) = B^2\xi^4 - 2Bm\xi^2 - A^2\xi^2 - 2A\Delta\xi + m^2 - \mu^2 - \Delta^2, \quad (A2)$$

$$F_2(\xi) = B^2\xi^4 - 2Bm\xi^2 - A^2\xi^2 + 2A\Delta\xi + m^2 - \mu^2 - \Delta^2. \quad (A3)$$

For $\mu = 0$, the quartic factors simplify to:

$$F_1(\xi) = (B\xi^2 - m - \Delta)(B\xi^2 + A\xi - m + \Delta), \quad (A4)$$

$$F_2(\xi) = (B\xi^2 - m + \Delta)(B\xi^2 - A\xi - m - \Delta), \quad (A5)$$

which can be solved exactly. For $\mu \neq 0$, we employ the approximations described in the main text to obtain the physically relevant solutions.

Appendix B: Detailed Derivation of Dispersion Relation

In the main text, we presented all edge states without explicitly specifying the normalization coefficient, which is necessary for calculating the dispersion relation. Therefore, we first calculate the normalization coefficient.

The wavefunction is given as:

$$\Psi(y) = \frac{1}{\sqrt{C}} (c_1 \mathbf{v}_1 e^{-\xi_1 y} + c_2 \mathbf{v}_2 e^{-\xi_2 y} + c_7 \mathbf{v}_7 e^{-\xi_7 y}). \quad (\text{B1})$$

where

$$c_1 = \frac{1 - \sigma}{2\sigma}, \quad c_2 = \frac{1 + \sigma}{2\sigma}, \quad c_7 = -1. \quad (\text{B2})$$

and

$$\mathbf{v}_1 = (\sigma, -1, -\sigma, 1)^T, \quad \mathbf{v}_2 = (\sigma, 1, -\sigma, -1)^T, \quad \mathbf{v}_7 = (1, 1, -1, -1)^T. \quad (\text{B3})$$

Using the normalization condition:

$$\int_0^\infty dy \Psi^\dagger(y) \Psi(y) = 1, \quad (\text{B4})$$

the normalization coefficient C is computed as:

$$\begin{aligned} C = & \frac{1}{\xi_1 + \xi_2^*} \left[1 - \frac{1}{2\sigma} - \frac{1}{2|\sigma|^2} - \frac{|\sigma|^2}{2} - \frac{\sigma}{2} + \frac{1}{2\sigma^*} + \frac{\sigma^*}{2} \right] \\ & + \frac{1}{\xi_2 + \xi_1^*} \left[1 + \frac{1}{2\sigma} - \frac{1}{2|\sigma|^2} - \frac{|\sigma|^2}{2} + \frac{\sigma}{2} - \frac{1}{2\sigma^*} - \frac{\sigma^*}{2} \right] \\ & + \frac{\xi_1}{\xi_1^2 + |\xi_1|^2} \left[1 - \frac{\sigma}{2} - \frac{1}{2\sigma} + \frac{|\sigma|^2}{2} - \frac{|\sigma|^2}{2\sigma} + \frac{1}{2|\sigma|^2} - \frac{1}{2\sigma^*} \right] \\ & + \frac{\xi_2}{\xi_2^2 + |\xi_2|^2} \left[1 + \frac{\sigma}{2} - \frac{1}{2\sigma} + \frac{|\sigma|^2}{2} - \frac{|\sigma|^2}{2\sigma} + \frac{1}{2|\sigma|^2} + \frac{1}{2\sigma^*} \right], \end{aligned} \quad (\text{B5})$$

which simplifies to:

$$C = \frac{2A(\Delta^2 + m\Delta + \mu^2)}{\Delta(\Delta^2 - m^2 + \mu^2)}. \quad (\text{B6})$$

Here, we have neglected terms involving ξ_7 , assuming that ξ_7 is very large and its contributions in denominators are negligible. Next, we calculate the perturbed energy for small k_x :

$$\begin{aligned} E(k_x) = & \int_0^\infty dy \Psi^\dagger(y) \mathcal{H}_1(k_x) \Psi(y) \\ = & \frac{Ak_x}{C} \frac{1}{\xi_1 + \xi_2^*} \left[1 - \frac{\sigma}{2} + \frac{1}{2\sigma} + \frac{\sigma^*}{2} - \frac{\sigma^*}{2\sigma} - \frac{\sigma^2}{2|\sigma|^2} + \frac{\sigma}{2|\sigma|^2} \right] \\ & + \frac{Ak_x}{C} \frac{1}{\xi_2 + \xi_1^*} \left[1 + \frac{\sigma}{2} - \frac{1}{2\sigma} - \frac{\sigma^*}{2} - \frac{\sigma^*}{2\sigma} - \frac{\sigma^2}{2|\sigma|^2} - \frac{\sigma}{2|\sigma|^2} \right] \\ & + \frac{Ak_x}{C} \frac{\xi_1}{\xi_1^2 + |\xi_1|^2} \left[1 - \frac{1}{2\sigma} - \frac{\sigma}{2} - \frac{|\sigma|^2}{2\sigma} + \frac{|\sigma|^2}{2\sigma^2} + \frac{\sigma^2}{2|\sigma|^2} - \frac{\sigma}{2|\sigma|^2} \right] \\ & + \frac{Ak_x}{C} \frac{\xi_2}{\xi_2^2 + |\xi_2|^2} \left[1 + \frac{1}{2\sigma} + \frac{\sigma}{2} + \frac{|\sigma|^2}{2\sigma} + \frac{|\sigma|^2}{2\sigma^2} + \frac{\sigma^2}{2|\sigma|^2} + \frac{\sigma}{2|\sigma|^2} \right]. \end{aligned} \quad (\text{B7})$$

After simplifications, this yields:

$$E(k_x) = \frac{\Delta(\Delta + m)}{\Delta^2 + m\Delta + \mu^2} Ak_x. \quad (\text{B8})$$

[1] E. Majorana, Nuovo Cim. **14**, 171 (1937).

[2] N. Read and D. Green, Physical Review B **61**, 10267

- (2000).
- [3] A. Y. Kitaev, *Phy. Usp.* **44**, 131 (2001).
- [4] L. Fu and C. L. Kane, *Phys. Rev. Lett.* **100**, 096407 (2008).
- [5] R. M. Lutchyn, J. D. Sau, and S. Das Sarma, *Phys. Rev. Lett.* **105**, 077001 (2010).
- [6] X.-L. Qi, T. L. Hughes, and S.-C. Zhang, *Phys. Rev. B* **82**, 184516 (2010).
- [7] T. D. Stanescu, J. D. Sau, R. M. Lutchyn, and S. Das Sarma, *Phys. Rev. B* **81**, 241310 (2010).
- [8] J. D. Sau, R. M. Lutchyn, S. Tewari, and S. Das Sarma, *Phys. Rev. B* **82**, 094522 (2010).
- [9] A. C. Potter and P. A. Lee, *Phys. Rev. B* **83**, 184520 (2011).
- [10] S. B. Chung, X.-L. Qi, J. Maciejko, and S.-C. Zhang, *Phys. Rev. B* **83**, 100512(R) (2011).
- [11] J. Alicea, *Rep. Prog. Phys.* **75**, 076501 (2012).
- [12] C. Beenakker, *Annu. Rev. Condens. Matter Phys.* **4**, 113 (2013).
- [13] S.-W. Li, Z.-Z. Li, C. Y. Cai, and C. P. Sun, *Phys. Rev. B* **89**, 134505 (2014).
- [14] J. Wang, Q. Zhou, B. Lian, and S.-C. Zhang, *Phys. Rev. B* **92**, 064520 (2015).
- [15] G.-J. Qiao, S.-W. Li, and C. P. Sun, *Phys. Rev. B* **106**, 104517 (2022).
- [16] X. Yue, G.-J. Qiao, and C. P. Sun, *Phys. Rev. B* **108**, 195405 (2023).
- [17] L. Chen, X.-H. Pan, Z. Cao, D. E. Liu, and X. Liu, *Phys. Rev. B* **109**, 075408 (2024).
- [18] G.-J. Qiao, X. Yue, and C. P. Sun, *Phys. Rev. Lett.* **133**, 266605 (2024).
- [19] X. Yue, G.-J. Qiao, and C. P. Sun, arXiv preprint 2506.16093 (2025).
- [20] G.-J. Qiao, Z.-L. Zhang, X. Yue, and C. P. Sun, arXiv preprint 2511.21423 (2025).
- [21] Z.-L. Zhang, G.-J. Qiao, and C. P. Sun, arXiv preprint arXiv:2506.10367 (2025).
- [22] G.-J. Qiao, X. Yue, Z.-L. Zhang, and C. P. Sun, *Acta Phys. Sin.* **75**, 6 (2026).
- [23] J. Osca and L. m. c. Serra, *Phys. Rev. B* **112**, 224519 (2025).
- [24] L. Huang, D. Qian, and J. Wang, *Phys. Rev. B* **113**, 014503 (2026).
- [25] V. Mourik, K. Zuo, S. M. Frolov, S. R. Plissard, E. P. A. M. Bakkers, and L. P. Kouwenhoven, *Science* **336**, 1003 (2012).
- [26] Q. L. He, L. Pan, A. L. Stern, E. C. Burks, X. Che, G. Yin, J. Wang, B. Lian, Q. Zhou, E. S. Choi, *et al.*, *Science* **357**, 294 (2017).
- [27] H. Zhang, C. Liu, S. Gazibegovic, D. Xu, J. A. Logan, G. J. Wang, N. van Loo, J. D. S. Bommer, M. W. A. de Moor, D. Car, *et al.*, *Nature* **556**, 74 (2018).
- [28] M. Kayyalha, D. Xiao, R. Zhang, J. Shin, and C. Z. Chang, *Science* **367**, 64 (2020).
- [29] A. Uday, G. Lippertz, K. Moors, *et al.*, *Nature Physics* **20**, 1589 (2024).
- [30] Y. Huang, Y. Fu, P. Zhang, K. L. Wang, and Q. L. He, *Journal of Physics: Condensed Matter* **36**, 37LT01 (2024).
- [31] A. Uday, G. Lippertz, B. Bhujel, A. A. Taskin, and Y. Ando, *Phys. Rev. B* **111**, 035440 (2025).
- [32] D. A. Ivanov, *Phys. Rev. Lett.* **86**, 268 (2001).
- [33] M. H. Freedman, M. J. Larsen, and Z. Wang, *Commun. Math. Phys.* **227**, 605 (2002).
- [34] A. Kitaev, *Ann. Phys.* **303**, 2 (2003).
- [35] C. Nayak, S. H. Simon, A. Stern, M. Freedman, and S. Das Sarma, *Rev. Mod. Phys.* **80**, 1083 (2008).
- [36] B. Lian, X.-Q. Sun, A. Vaezi, X.-L. Qi, and S.-C. Zhang, *Proceedings of the National Academy of Sciences* **115**, 10938 (2018).
- [37] C. Reeg, D. Loss, and J. Klinovaja, *Phys. Rev. B* **96**, 125426 (2017).
- [38] C. Reeg, D. Loss, and J. Klinovaja, *Phys. Rev. B* **97**, 165425 (2018).
- [39] H. F. Legg, D. Loss, and J. Klinovaja, *Phys. Rev. B* **105**, 155413 (2022).
- [40] B. Zhou, H.-Z. Lu, R.-L. Chu, S.-Q. Shen, and Q. Niu, *Phys. Rev. Lett.* **101**, 246807 (2008).
- [41] J. Linder, T. Yokoyama, and A. Sudbø, *Phys. Rev. B* **80**, 205401 (2009).
- [42] S.-Q. Shen, *Topological Insulators: Dirac Equation in Condensed Matters*, Springer Series in Solid-State Sciences, Vol. 174 (Springer, 2012).
- [43] M. König, H. Buhmann, L. W. Molenkamp, T. Hughes, C.-X. Liu, X.-L. Qi, and S.-C. Zhang, *Journal of the Physical Society of Japan* **77**, 031007 (2008), <https://doi.org/10.1143/JPSJ.77.031007>.
- [44] M. Z. Hasan and C. L. Kane, *Rev. Mod. Phys.* **82**, 3045 (2010).
- [45] X. Liu, Q.-f. Sun, and X. C. Xie, *Phys. Rev. B* **85**, 235459 (2012).
- [46] R. Yu, W. Zhang, H.-J. Zhang, S.-C. Zhang, X. Dai, and Z. Fang, *Science* **329**, 61 (2010).
- [47] W.-Y. Shan, H.-Z. Lu, and S.-Q. Shen, *New J. Phys.* **12**, 043048 (2010).
- [48] B. I. Halperin, *Phys. Rev. B* **25**, 2185 (1982).
- [49] F. D. M. Haldane, *Phys. Rev. Lett.* **61**, 2015 (1988).